УДК 537.525
P.A.C.S. 52.80.

DOI 10.54708/26587572_2023_5414146

FEATURES OF TITANIUM ION BEAMS FORMATION TAKING INTO ACCOUNT ION-ELECTRON EMISSION REALIZING THE SYNERGY OF HIGH-INTENSITY ION IMPLANTATION AND PULSED ENERGY IMPACT ON THE SURFACE

Dimitrii Olegovich Vakhrushev [a], *Sergey Valentinovich Dektyarev, Olga Sergeevna Korneva*

Tomsk Polytechnic University, Lenin pr. 2, bldg. 4, 634028, Tomsk, Russia
[a] dov3@tpu.ru

ABSTRACT

In this work, we show the possibility of forming titanium ion beams of submillisecond duration in the average ion energy range from 20 to 60 keV with a maximum ion current density of 3.3 A/cm^2 at a pulsed power density of 132 kW/cm^2 in individual pulses. The dependence of the ion-electron emission coefficient on the average energy and current of the arc discharge is presented. It has been established that the ion-electron emission coefficient in the case of irradiation of a stainless steel target with a beam of titanium ions reaches a value of 1.6 at an average ion energy of 60 keV. The dependences of the radial distribution of the ion current density on the average ion energy are obtained for different positions of the collector relative to the geometric focus of the ballistic system for focusing the ion beam. Taking into account ion-electron emission, it has been experimentally shown that with an increase in the average ion energy from 20 keV to 40 keV, an increase in the density of the measured ion current is observed, while in the range from 40 to 60 keV, the ion current density decreases. Using nineteen collector sensors, it was shown that due to the influence of the partially uncompensated space charge of the ion beam, the best conditions for its focusing are achieved at a distance of 20 mm behind the geometric focus of the system.

KEYWORDS

Ion-electron emission; energy impact; high-intensity ion beams.

ОСОБЕННОСТИ ФОРМИРОВАНИЯ ПУЧКОВ ИОНОВ ТИТАНА С УЧЕТОМ ИОННО-ЭЛЕКТРОННОЙ ЭМИССИИ, ПРИ КОТОРОМ РЕАЛИЗУЕТСЯ СИНЕРГИЯ ВЫСОКОИНТЕНСИВНОЙ ИОННОЙ ИМПЛАНТАЦИИ И ИМПУЛЬСНОГО ЭНЕРГЕТИЧЕСКОГО ВОЗДЕЙСТВИЯ НА ПОВЕРХНОСТЬ

Дмитрий Олегович Вахрушев [a], *Сергей Валентинович Дектярев , Ольга Сергеевна Корнева*

Томский политехнический университет, Россия, 634028, Томск, пр. Ленина, 2, стр. 4
[a] dov3@tpu.ru

АННОТАЦИЯ

В данной работе показана возможность формирования пучков ионов титана субмиллисекундной длительности в диапазоне средних энергий ионов от 20 до 60 кэВ с максимальной плот-

ностью ионного тока 3,3 А/см^2 при плотности импульсной мощности 132 кВт/см^2 в отдельных импульсах. Представлена зависимость коэффициента ионно-электронной эмиссии от средней энергии и тока дугового разряда. Установлено, что коэффициент ионно-электронной эмиссии при облучении мишени из нержавеющей стали пучком ионов титана достигает значения 1,6 при средней энергии ионов 60 кэВ. Получены зависимости радиального распределения плотности ионного тока от средней энергии ионов для различных положений коллектора относительно геометрического фокуса баллистической системы для фокусировки ионного пучка. С учетом ионно-электронной эмиссии экспериментально показано, что при увеличении средней энергии ионов с 20 кэВ до 40 кэВ наблюдается увеличение плотности измеряемого ионного тока, а в диапазоне от 40 до 60 кэВ плотность ионного тока уменьшается. С помощью девятнадцати датчиков-коллекторов было показано, что за счет влияния частично некомпенсированного объемного заряда ионного пучка наилучшие условия для его фокусировки достигаются на расстоянии 20 мм за геометрическим фокусом системы.

КЛЮЧЕВЫЕ СЛОВА

Ионно-электронная эмиссия; энергетическое воздействие; ионные пучки высокой интенсивности.

Introduction

With the development of production, the requirements for modern materials increase. The main factor limiting the service life of complex science-intensive products, today, is the destruction of the surface layers of materials. In this regard, methods of modifying the surface of materials are of interest. Such methods include the application of wear-resistant coatings, for example, by plasma or arc spraying [1–3]. At the same time, it is possible to spray both metal [4] and composite [5] and even ceramic coatings [6]. However, the quality of the resulting coatings (adhesion strength, wear resistance of the coating) is affected by a number of factors, for example, the state of the substrate surface or the reaction of elements at the interface between the coating and substrate materials, which limit the scope of the method of applying wear-resistant coatings [7]. To date, there are also a large number of promising methods of beam and plasma technologies for modifying the surface layers of materials, such as electron beam processing [8–10], laser irradiation [11–15], exposure to compression plasma flows [16–20]. The common advantage of such methods is the ultra-high rate of surface heating up to the melting temperature and subsequent cooling of the surface layer of the material due to heat removal to the main volume of the material at a cooling rate of up to 10^9 K/s, which contributes to the effect of material hardening and the formation of a submicro- and nanosized homogeneous structure. A common disadvantage of such methods is the dissolution of the functional structures of heterogeneous systems that provide certain properties, which leads to a deterioration in the properties of the system itself [21, 22].

An alternative method for modifying the surface of materials is the ion implantation method. The advantage of the method is the possibility of modifying a wide range of materials, such as metals, semiconductors and even dielectrics, and the modification occurs due to changes in the elemental and phase composition of the material being processed. The main problem of the ion implantation method associated with small impurity doping depths was solved for semiconductor materials in the framework of high-energy ion implantation with an ion energy of tens to hundreds of meV [23]. From the point of view of metal processing, the low sensitivity to the presence of impurities predetermined the need to increase the dose of ion irradiation by several orders

of magnitude compared to semiconductors to levels of 10^{17}–10^{18} ion/cm^2. The possibilities of conventional ion implantation are limited by the projective ranges of ions in the material at the level of tens of nanometers. To solve this problem, a method of high-intensity ion implantation was proposed, aimed at stimulating radiation diffusion, which makes it possible to obtain doped layers with a thickness of tens to hundreds of micrometers [24]. At the same time, a set of studies performed showed that in some cases, significant heating of the entire matrix layer during irradiation is required, which leads to the growth of the grain structure [25, 26]. In this regard, in [27, 28], a method was proposed based on the synergy of high-intensity ion implantation and pulsed energy impact on the material surface by submillisecond ion beams. Simultaneous implantation of ions and their energy impact on the surface layer will provide not only deep ion doping, but also an improvement in the microstructure due to the repetitively pulsed effect of superhardening of the ion-doped layer. This approach will make it possible to exclude the heating of the entire matrix layer to high temperatures, at which the deterioration of the microstructure of materials occurs. To implement the method, beams with a pulsed power density of hundreds of kilowatts per square centimeter are required.

This work is devoted to the features of the formation of repetitively pulsed beams of submillisecond titanium ions with a high power density. Particular attention is paid to the study of ion-electron emission, which affects both the neutralization of the space charge of long-pulse beams and the accuracy of measuring the ion current density and the power density of the ion beam.

1. Research methodology

The study on the formation of titanium ion beams consisted of several stages: 1) measuring the current near the output of the plasma generator with a collector diameter of 285 mm; 2) measurement of the ion current density near the geometric focus of the ion beam formation system, the area of which was about 7 mm^2, by nineteen sensors. The first stage was carried out to evaluate the ion-electron emission from the collector surface. The second stage made it possible to determine the distribution profile of the ion current density over the beam cross section.

Experimental studies were carried out on a complex installation equipped with a modified Raduga-5 ion source, Fig. 1. The vacuum-arc evaporator (1) generated titanium plasma in a continuous mode at arc discharge currents of 130 A and 170 A. A grid electrode (3) was used to extract ions from the plasma in the form of a part of a sphere with a radius of curvature of 130 mm, located along the axis of the plasma generator inside the vacuum chamber (4). The extracting grid electrode had a grid cell size of 1.1×1.2 mm with a transparency of 60.4%. To cut off the deposition of the microdroplet fraction of the vacuum-arc discharge on the irradiated surface, a disk electrode (2) located along the axis of the ion source was used. The formation of ion beams was carried out in a repetitively pulsed mode using pulsed voltage generators (6), with an amplitude from 0.1 kV to 30 kV. One of the generators at an accelerating voltage pulse frequency of 1 kHz in the amplitude range of 0.1–1.8 kV provided a pulse duration of 100 μs. The second generator, at a pulse frequency of 10 Hz, provided an accelerating voltage amplitude in the range of 5–30 kV at a pulse duration of 450 μs. In order to obtain statistically reliable results, the oscillograms were averaged over 1024 pulses at an accelerating voltage of 0.1–1.8 kV and over 384 pulses at an accelerating voltage from 5 to 30 kV. Averaging was carried out using the mathematical apparatus of the Rigol MSO5000 oscilloscope. The collector unit (5) consisting of nineteen sensors was installed in different positions relative to the geometric focus of the beam formation system.

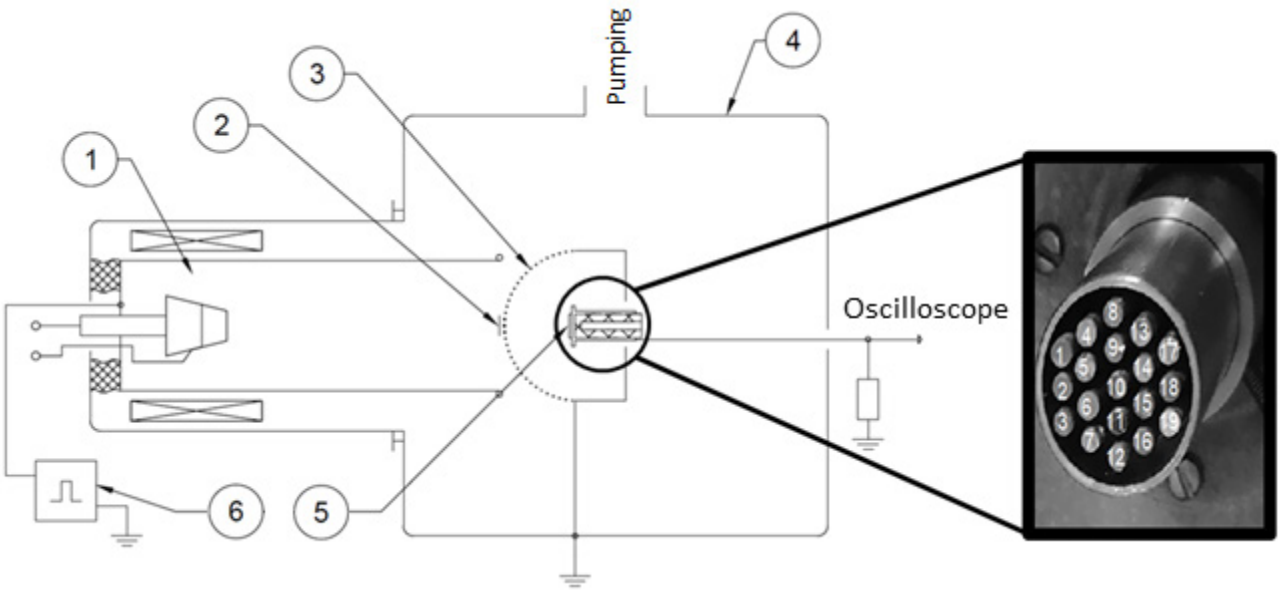

Fig. 1. Scheme of the experimental setup

Рис. 1. Схема экспериментальной установки

2. Results and discussion

To estimate the ion-electron emission during titanium plasma generation at arc discharge currents of 130 A and 170 A, the current amplitudes on a solid flat collector were measured, depending on the accelerating voltage, Fig. 2. Fig. 2, *a* shows that the amplitude ranges of the accelerating voltage are 0.1–1.8 kV corresponds to an initial collector current of 1.43 A and 2.85 A at arc discharge currents of 130 A and 170 A, respectively. It can be noted that an increase in the discharge current by 30% led to an increase in the collector current by a factor of two. This fact is explained by the design features that change the configuration of the magnetic fields of the coil depending on the arc discharge current, Fig. 1. The currents measured at low accelerating voltages are ion saturation currents from the vacuum arc plasma.

Increasing the amplitude of the accelerating voltage from 0.1 kV to 0.4 kV (Fig. 2, *a*) does not change the amplitude of the ion current. A further increase in the accelerating voltage amplitude leads to a gradual increase in the current amplitude, which is associated with the appearance of ion-electron emission.

The ion-electron emission coefficient can be determined from the dependences of the collector current on the average ion energy. The product of the average charge state of titanium ions (about two) and the amplitude of the accelerating voltage determines the average energy of titanium ions in a continuous plasma of a vacuum arc. Fig. 3 shows a graph of the dependence of the ion-electron emission coefficient on the average ion energy at arc discharge currents of 130 A and 170 A. The data in the figure show that the ion-electron emission coefficient in this current range does not depend on the discharge current of the arc evaporator. The maximum value of the coefficient of ion-electron emission of a titanium ion beam on a stainless steel target reaches 1.6 at an average ion energy of 60 keV.

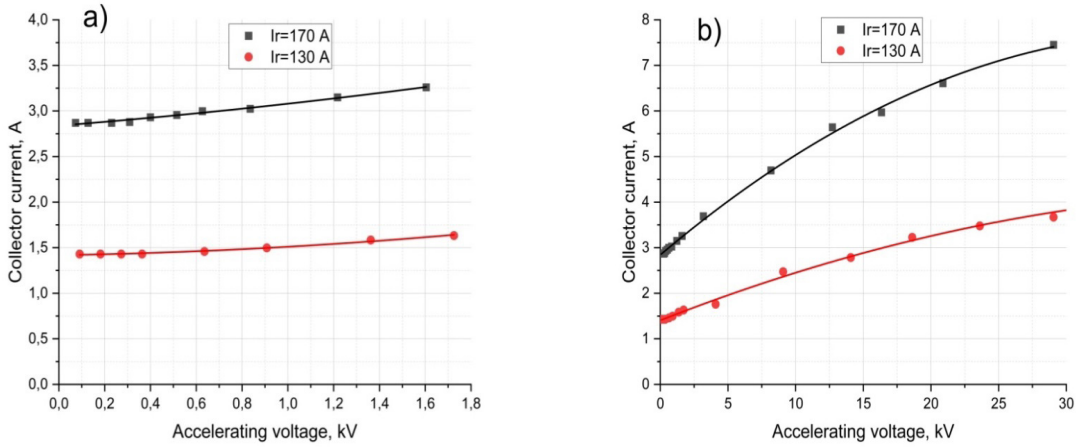

Fig. 2. The current on the collector depending on the accelerating voltage:
a – in the region of 0.1 kV–1.8 kV; b – in the region of 0.1 kV–30 kV at arc discharge currents of 130 A and 170 A

Рис. 2. Ток на коллекторе в зависимости от ускоряющего напряжения:
а – в области 0,1 кВ–1,8 кВ; b – в области 0,1 кВ–30 кВ при токах дугового разряда 130 А и 170 А

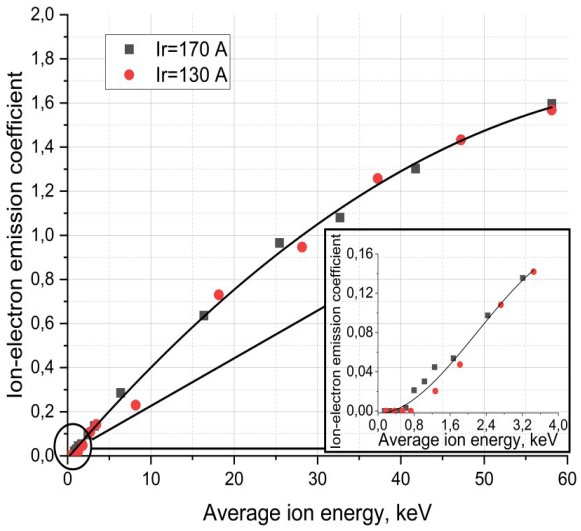

Fig. 3. Dependence of the ion-electron emission coefficient on the accelerating voltage at arc currents of 130 A and 170 A

Рис. 3. Зависимость коэффициента ионно-электронной эмиссии от ускоряющего напряжения при токах дугового разряда 130 А и 170 А

The next step was to conduct a series of experiments on focusing the titanium ion beam using an extracting electrode, Fig. 1. The studies were aimed at studying the influence of the average ion energy, the location of the collector unit relative to the geometric focus of the beam formation system, and the arc discharge current on the beam ion current density distribution profile.

The studies were carried out using nineteen sensors located inside a circle with a diameter of 22 mm, Fig. 1. Each of the sensors was isolated from the others using a dielectric holder. Fig. 4 shows current density measurements recorded by nineteen collectors at a distance of 20 mm behind the geometric focus of the beam focusing system at an average ion energy of 40 keV.

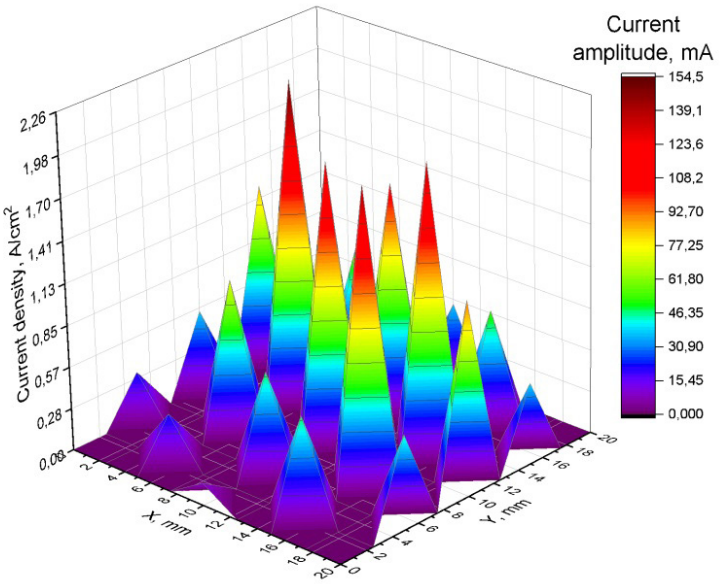

Fig. 4. Current on the collector node of nineteen isolated sensors

Рис. 4. Ток на коллекторном узле из девятнадцати изолированных датчиков

On the basis of experimental data obtained, a profile of the distribution of the current density of titanium ions over the beam cross section was constructed, taking into account ion-electron emission, depending on the position of the end part of the collector assembly relative to the geometric focus of the formation system from –10 mm to +30 mm with a step of 10 mm, Fig. 5. In this case, the average ion energy and the arc discharge current remained fixed and amounted to 40 keV and 130 A, respectively. Fig. 5, *a* shows the 3D distribution of the ion current density profiles over the beam cross section in space. It can be estimated qualitatively that, moving away from the geometric focus of the beam formation system, the conditions for its transportation first improve in the region from F–10 mm to F+20 mm, as indicated by an increase in the amplitude of the ion current density. A further shift from the geometric focus of the system to the region F+30 mm leads to a decrease in the amplitude of the ion current density, which indicates beam defocusing. Previously, a similar effect was observed in the generation of low-energy silicon ion beams [29]. Based on the data in Fig. 5, *b*, the amplitude of the ion current density can be quantified. Thus, the smallest amplitude of the ion current density of 0.29 A/cm^2 was recorded at a distance of 10 mm in front of the geometric focus of the beam formation system. The best conditions for beam focusing and transport took place in the F+20 mm region, where the maximum amplitude of the ion current density was 0.95 A/cm^2, which corresponds to a beam power density of 38 kW/cm^2 in each pulse. The distance of the collector node to the region F+30 mm contributed to the decrease in the amplitude of the ion current density to 0.83 A/cm^2. An interesting point is the fact that when the collector unit is dynamically moved from the F–10 mm region to the F+10 mm region, the beam width at half-height decreases with an increase in the ion current density amplitude. A further shift to the F+20 mm region leads not only to an increase in the ion current density, but also to a broadening of the current density distribution over the beam cross section, which may indicate the onset of beam defocusing processes. Thus, it can be assumed that the best condition for focusing and transporting the ion beam is in the area of the collector position between F+10 mm and F+20 mm.

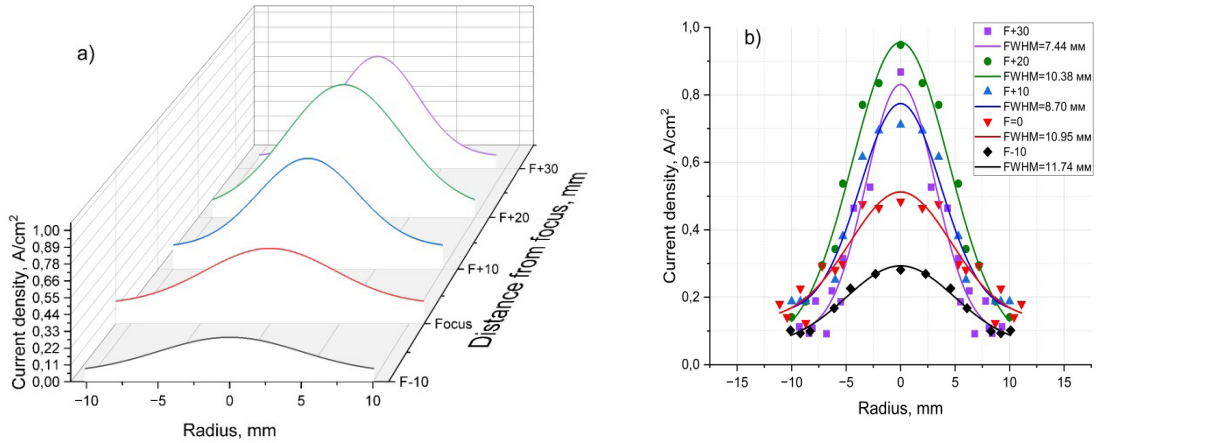

Fig. 5. The current density distribution profile of the collectors over the beam cross section depending on the position of the end part of the collector assembly relative to the geometric focus of the beam formation system:
a – 3D profile; b – 2D profile at an accelerating voltage of 40 keV and an arc discharge current of 130 A

Рис. 5. Профиль распределения плотности тока коллекторов по сечению пучка в зависимости от положения торцевой части коллекторного узла относительно геометрического фокуса системы формирования пучка:
a – 3Д профиль; b – 2Д профиль при ускоряющем напряжении 40 кэВ и токе дугового разряда 130 А

The distribution profile of the current density of the collectors over the beam cross section depending on the average energy of the ions, taking into account ion-electron emission, is shown in Fig. 6. In this case, the position of the end part of the collector assembly relative to the geometric focus of the beam formation system and the arc discharge current remained fixed and amounted to F+20 mm and 130 A respectively. It can be seen from the figure that an increase in the average ion energy from 20 keV to 40 keV leads to an increase in the amplitude of the ion current density. A further increase in the average ion energy leads to a decrease in the amplitude of the ion current density to a minimum value of 0.76 A/cm^2. The decrease in the amplitude of the ion current density over the beam cross section upon passing from the average ion energy of 40 keV to 60 keV was first theoretically predicted in [27]. By simulating the process of passage of ions through the grid extractor using the KARAT code, the authors showed the possibility of violating the conditions of equipotentiality of the beam drift space due to the possibility of plasma electrons escaping through the cells of the grid extractor, entrained by the electric field. In this case, the space charge neutralization conditions are violated, which may indicate the fact of a decrease in the amplitude of the ion current density on the collectors.

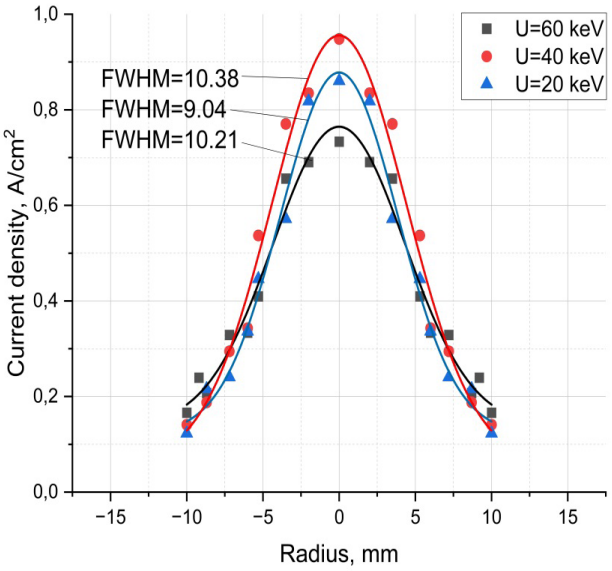

Fig. 6. The current density distribution profile of the collectors over the beam cross section as a function of the accelerating voltage in the region where the end part of the collector assembly is located 20 mm behind the focus and the arc discharge current is 130 A

Рис. 6. Профиль распределения плотности тока коллекторов по сечению пучка в зависимости от ускоряющего напряжения в области расположения торцевой части коллекторного узла 20 мм за фокусом и токе дугового разряда 130 А

The parameter of the full beam width at the half-maximum height FWHM in the target irradiation mode at an average ion energy of 40 keV was about 10 mm, which corresponds to the diameter of the beam imprint on a stainless steel metal plate, which was irradiated in the same mode with a long exposure to the beam, Fig. 7.

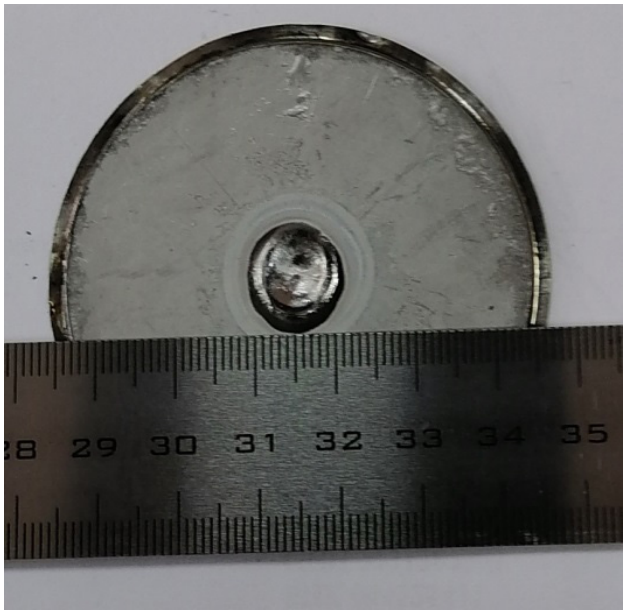

Fig. 7. Ion beam imprint on stainless steel after prolonged exposure

Рис. 7. Отпечаток пучка ионов на нержавеющей стали после длительного воздействия

To study the influence of the arc current on the ion current density, the arc discharge current was increased to 170 A. The average ion energy and the position of the collector relative to the geometric focus of the beam formation system remained constant and amounted to 40 keV and F+20 mm, respectively. Fig. 8 shows the distribution profiles of the ion current density at arc discharge currents of 130 A (1) and 170 A (2) averaged and a single, close to maximum, pulse at an arc discharge current of 170 A (3), taking into account ion-electron emission corresponding to given value of the average ion energy. An increase in the arc discharge current to 170 A contributed to an increase in the ion current density to 1.47 A/cm^2, which corresponds to a beam power density approaching 60 kW/cm^2. In this case, it is interesting to consider single pulses, the amplitude of the ion current density of which reaches 3.3 A/cm^2 or the impulse beam power density of 132 kW/cm^2, which is 2.2 times higher than the averaged ones. It is important to focus on the fact that when modifying materials under conditions of synergy of irradiation with high-intensity ion beams and energy exposure, the greatest contribution will be made by pulses of maximum power density. In this regard, in further studies, it will be interesting to evaluate the quantitative distribution of pulses by energy power density instead of averaged pulses.

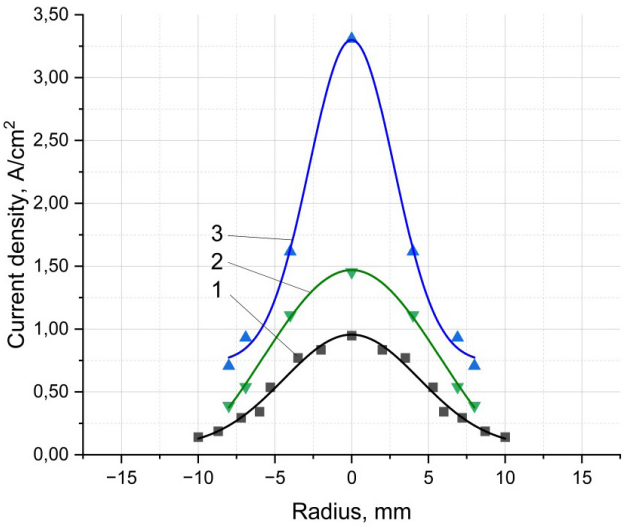

Fig. 8. Collector ion current density distribution profiles at arc discharge currents of 1) 130 A and 2) 170 A averaged over sixteen pulses and 3) a single pulse at an arc discharge current of 170 A

Рис. 8. Профили распределения плотности ионного тока коллектора при токах дугового разряда 1) 130 А и 2) 170 А с усреднением по шестнадцати импульсам и 3) одиночный импульс при токе дугового разряда 170 А

To estimate the total ion current, the currents of all collectors were summed, taking into account ion-electron emission. Thus, for the case of an arc discharge current of 130 A, an average ion energy of 40 keV, and the location of the end part of the collector assembly at a position of F + 20 mm from the geometric focus of the beam formation system, the total ion current was determined to be 0.59 A. It is

noteworthy that for an arc discharge current of 130 A, the maximum possible current extracted from the Raduga-5 system is 1.43 A. Taking into account the transparency of the grid extraction electrode, the maximum possible current of the system is 0.86 A. Then, up to 46% is lost during beam transportation.

Conclusions

In this work, the ion-electron emission coefficient was experimentally determined depending on the average ion energy up to 60 keV. The features of the formation of titanium ion beams generated by the modified Raduga-5 ion source at accelerating voltage amplitudes from 0.1 kV to 30 kV and arc discharge currents of 130 A and 170 A were demonstrated for the first time. The dependence of the amplitude of the ion current density during dynamic displacement of the collector unit relative to the geometric focus of the ion beam formation system is shown. The possibility of forming submillisecond titanium ion beams with a maximum ion current density of 3.3 A/cm^2 and a beam power density of 132 kW/cm^2 with allowance for ion-electron emission is shown.

Acknowledgments / Благодарности

The study was supported by the Russian Science Foundation, grant No. 22-19-00051.

Исследование было поддержано Российским Научным фондом грант № 22-19-00051.

REFERENCES

1. Wang Q., Rui X., Wang Q.-J., Bai Y., Du Zh.-Z., Niu W.-J., Wang W., Wang K.-S., Gao Y. Bonding and wear behaviors of supersonic plasma sprayed Fe-based coatings on Al-Si alloy substrate // Surface and Coatings Technology. 2019. V. 367. P. 288–301. DOI: 10.1016/j.surfcoat.2019.04.003.

2. Jang M. S., Ma S. W., Song J., Sung M., Kim Y.-H. Adhesion of NCF to oxidized Si wafers after oxygen plasma treatment // Microelectronics Reliability. 2017. V. 78. P. 220–226. DOI: 10.1016/j.microrel.2017.09.001.

3. Farag O. F. Comparison of the effect of plasma treatment and gamma ray irradiation on PS-Cu nanocomposite films surface // Results in Physics. 2018. V. 9. P. 91–99. DOI: 10.1016/j.rinp.2018.02.031.

4. Hejwowski T. Sliding wear resistance of Fe-, Ni- and Co-based alloys for plasma deposition // Vacuum. 2006. V. 80, Iss. 11–12. P. 1326–1330. DOI: 10.1016/j.vacuum.2006.01.037.

5. He L., Tan Y., Wang X., Xu T., Hong X. Microstructure and wear properties of Al_2O_3-CeO_2/Ni-base alloy composite coatings on aluminum alloys by plasma spray // Applied Surface Science. 2014. V. 314. P. 760–767. DOI: 10.1016/j.apsusc.2014.07.047.

6. He P., Ma G., Wang H., Yong Q., Chen S., Xu B. Tribological behaviors of internal plasma sprayed TiO_2-based ceramic coating on engine cylinder under lubricated conditions // Tribology international. 2016. V. 102. P. 407–418. DOI: 10.1016/j.triboint.2016.06.011.

7. Hwang B., Lee S., Ahn J. Effect of oxides on wear resistance and surface roughness of ferrous coated layers fabricated by atmospheric plasma spraying // Materials Science and Engineering A. 2002. V. 335, Iss. 1–2. P. 268–280. DOI: 10.1016/S0921-5093(01)01937-2.

8. Wei D., Wang X., Wang R., Cui H. Surface modification of 5CrMnMo steel with continuous scanning electron beam process // Vacuum. 2018. V. 149. P. 118–123. DOI: 10.1016/j.vacuum.2017.12.032.

9. Tao X., Yao Zh., Zhang Sh., Liao J., Liang J. Investigation on microstructure, mechanical and tribological properties of in-situ (TiB+ TiC)/Ti composite during the electron beam surface melting // Surface and Coatings Technology. 2018. V. 337. P. 418–425. DOI: 10.1016/j.surfcoat.2018.01.054.

10. Ivanov Yu. F., Gromov V. E., Konovalov S. V., Zagulyaev D. V., Semin A. P. Formation of structure and properties of silumin on electron-beam processing // Journal of Surface Investigation: X-ray, Synchrotron and Neutron Techniques. 2019. V. 13. P. 1040–1044. DOI: 10.1134/S1027451019060090.

11. Kang N., Mansori M. E. L. A new insight on induced-tribological behaviour of hypereutectic Al-Si alloys manufactured by selective laser melting // Tribology International. 2020. V. 149. Article number 105751. DOI: 10.1016/j.triboint.2019.04.035.

12. Mahanty S., Gouthama. Surface modification of Al–Si alloy by excimer laser pulse processing // Materials Chemistry and Physics. 2016. V. 173. P. 192–199. DOI: 10.1016/j.matchemphys.2016.02.001.

13. Viswanathan A., Sastikumar D., Kumar H., Nath A. K. Laser processed TiC–$Al_{13}Fe_4$ composite layer formation on Al–Si alloy // Optics and Lasers in Engineering. 2012. V. 50, Iss. 9. P. 1321–1329. DOI: 10.1016/j.optlaseng.2012.02.013.

14. Oliveira V., Sharma S. P., de Moura M. F. S. F., Moreira R. D. F., Vilar R. Surface treatment of CFRP composites using femtosecond laser radiation // Optics and Lasers in Engineering. 2017. V. 94. P. 37–43. DOI: 10.1016/j.optlaseng.2017.02.011.

15. Ahuir-Torres J. I., Arenas M. A., Perrie W., de Damborenea J. Influence of laser parameters in surface texturing of Ti6Al4V and AA2024-T3 alloys // Optics and Lasers in Engineering. 2018. V. 103. P. 100–109. DOI: 10.1016/j.optlaseng.2017.12.004.

16. Uglov V., Anishchik V. M., Astašynski V., Sveshnikov Yu. V. Changes in the microstructure and mechanical properties of iron as a result of exposure to a compressive plasma flow // Physics and chemistry of material processing. 2004. V. 4. P. 37–42.

17. Anishchik V. M., Uglov V. V., Astashynski V. V., Astashynski V. M., Ananin S. I., Kostyukevich E. A., Kuzmitski A. M., Kvasov N. T., Danilyuk A. L., Rumianceva I. N. Compressive plasma flows interaction with steel surface: structure and mechanical properties of modified layer // Vacuum. 2003. V. 70, Iss. 2–3. P. 269–274. DOI: 10.1016/S0042-207X(02)00654-1.

18. Uglov V. V., Anishchik V. M., Astašynski V., Sveshnikov Yu. V., Rumyantseva I. N., Astashynski V. M., Ananin S. I., Askerko V. V., Kostyukevich E. A., Kuz'mitskij A. M., Kvasov N. T., Danilyuk A. L. Modification of the structure and properties of the surface layers of carbon steels when exposed to compression plasma flows // Physics and chemistry of material processing. 2002. V. 3. P. 23–28.

19 Astashinsky V. M., Ananin S. I. Influence of compression plasma flows on carbon steel and silicon // Vacuum technique and technology. 2002. V. 12, Iss. 2. P. 91–94.

20. Cherenda N. N., Uglov V. V., Anishchik V. M., Stalmashonak A. K., Astashinski V. M., Kuzmickii A. M., Punko A. V., Thorwath G., Stritzker B. Modification of high-speed steels by nitrogen compression plasma flow: Structure, element composition, tribological properties // Surface and coatings technology. 2006. V. 200, Iss. 18–19. P. 5334–5342. DOI: 10.1016/j.surfcoat.2005.06.007.

21. Han M., Landry F., Lieb K.-P., Schaaf P. Analysis of laser-nitrided stainless steel via nuclear methods // Applied Physics A. 1999. V. 69. P. S795–S797. DOI: 10.1007/s003399900247.

22. Mei X., Hao Sh., Ma T., Wang Y., Liu Zh. Microstructure and wear resistance of high-speed steel treated with intense pulsed ion beam // Nuclear Instruments and Methods in Physics, Research Section B: Beam Interactions with Materials and Atoms. 2005. V. 239, Iss. 3. P. 152–158. DOI: 10.1016/j.nimb.2005.03.292.

23. Komarov F. F. Ion implantation in metals. Moscow: Metallurgy, 1990. P. 216.

24. Ryabchikov A. I., Sivin D. O., Anan'in P. S., Ivanova A. I., Uglov V. V., Korneva O. S. DIN 1.7035 Steel Modification with High Intensity Nitrogen Ion Implantation // Russian Physics Journal. 2018. V. 61, Iss. 2. P. 270–277. DOI: 10.1007/s11182-018-1397-3.

25. Ryabchikov A. I., Shevelev A. E., Sivin D. O., Bozhko I. A., Kashkarov E. B., Bleykher G. A., Stepanov I. B., Ivanova A. I. Ultra high fluence implantation of aluminum ions into CP-Ti // Journal of Alloys and Compounds. 2019. V. 793. P. 604–612. DOI: 10.1016/j.jallcom.2019.04.179.

26. Ryabchikov A. I., Kashkarov E. B., Pushilina N. S., Syrtanov M. S., Shevelev A. E., Korneva O. S., Sutygina A. N., Lider A. M. High-intensity low energy titanium ion implantation into zirconium alloy // Applied Surface Science. 2018. V. 439. P. 106–112. DOI: 10.1016/j.apsusc.2018.01.021.

27. Ryabchikov A. I., Tarakanov V. P., Korneva O. S., Sivin D. O., Gurulev A. V. Simulation and experimental studies on the formation of high-power titanium ion beams for the synergy of ion implantation and energy impact on the surface // Nuclear Instruments and Methods in Physics, Research Section B: Beam Interactions with Materials and Atoms. 2022. V. 533. P. 29–39. DOI: 10.1016/j.nimb.2022.10.015.

28. Ryabchikov A. I., Dektyarev S. V., Korneva O. S., Vakhrushev D. O. Formation of High-Power Pulsed Titanium Ion Beams of Submillisecond Duration from Vacuum Arc Plasma // Russian Physics Journal. 2023. V. 65, Iss. 4. P. 1940–1946. DOI: 10.1007/s11182-023-02854-y.

29. Ryabchikov A. I., Sivin D. O., Dektyarev S. V., Shevelev A. E. Formation of repetitively pulsed high-intensity, low-energy silicon ion beams // Nuclear Instruments and Methods in Physics, Research Section A: Accelerators, Spectrometers, Detectors and Associated Equipment. 2020. V. 953. Article number 163092. DOI: 10.1016/j.nima.2019.163092.